

Assessment of Material By-Product Fate from Bioresorbable Vascular Scaffolds

TAREK SHAZLY,¹ VIJAYA B. KOLACHALAMA,² JAHID FERDOUS,¹ JAMES P. OBERHAUSER,³ SYED HOSSAINY,³
and ELAZER R. EDELMAN^{2,4}

¹College of Engineering and Computing, Department of Mechanical Engineering and Biomedical Engineering, University of South Carolina, Columbia, SC 29208, USA; ²Harvard-MIT Division of Health Sciences and Technology, Massachusetts Institute of Technology, Cambridge, MA 02139, USA; ³Abbott Vascular, Santa Clara, CA 95054, USA; and ⁴Cardiovascular Division, Brigham and Women's Hospital, Harvard Medical School, Boston, MA 02115, USA

(Received 27 June 2011; accepted 10 October 2011; published online 26 October 2011)

Associate Editor Kent Leach oversaw the review of this article.

Abstract—Fully bioresorbable vascular scaffolds (BVS) are attractive platforms for the treatment of ischemic artery disease owing to their intrinsic ability to uncage the treated vessel after the initial scaffolding phase, thereby allowing for the physiological conditioning that is essential to cellular function and vessel healing. Although scaffold erosion confers distinct advantages over permanent endovascular devices, high transient by-product concentrations within the arterial wall could induce inflammatory and immune responses. To better understand these risks, we developed in this study an integrated computational model that characterizes the bulk degradation and by-product fate for a representative BVS composed of poly(L-lactide) (PLLA). Parametric studies were conducted to evaluate the relative impact of PLLA degradation rate, arterial remodeling, and metabolic activity on the local lactic acid (LA) concentration within arterial tissue. The model predicts that both tissue remodeling and PLLA degradation kinetics jointly modulate LA fate and suggests that a synchrony of these processes could minimize transient concentrations within local tissue. Furthermore, simulations indicate that LA metabolism is a relatively poor tissue clearance mechanism compared to convective and diffusive transport processes. Mechanistic understanding of factors governing by-product fate may provide further insights on clinical outcome and facilitate development of future generation scaffolds.

Keywords—Bioresorbable vascular scaffolds, Ischemic artery disease, Computational modeling, Poly(L-lactide), Lactic acid.

Address correspondence to Tarek Shazly, College of Engineering and Computing, Department of Mechanical Engineering and Biomedical Engineering, University of South Carolina, Columbia, SC 29208, USA. Electronic mail: shazly@enr.sc.edu

Tarek Shazly and Vijaya B. Kolachalama contributed equally in this study.

INTRODUCTION

Percutaneous coronary intervention (PCI) has transformed clinical cardiovascular medicine. Polymer-coated, metallic drug-eluting stents (DES) serve as permanent implants that prevent vessel re-narrowing and control the release of antiproliferative pharmacological compounds intended to attenuate the neointimal hyperplastic response. However, issues related to incomplete vessel healing characterized by poor re-endothelialization, stent thrombosis, and late clinical fatalities create concerns about the long-term effects of metallic-based stent platforms.^{11,12,15} Emerging technologies attempting to mitigate these risks are now gaining impetus, and in particular, bioresorbable vascular scaffold (BVS) composed of fully resorbable polymers are being evaluated pre-clinically and clinically across various vascular beds.^{6,13} While BVS platforms demonstrate a clear potential to mitigate risk stemming from incomplete vessel healing, they introduce a new set of considerations to clinical safety and efficacy. Foremost among these issues is the fate of and biological response to material by-products that evolve throughout the scaffold degradation and resorption processes. Several studies have quantified biodegradable material behavior *in vitro* and *in vivo*,^{19,23,32} but the physical and chemical factors that govern by-product fate and associated biological response are difficult to be quantified in traditional experimental settings.

Computational modeling offers an efficient framework to predict and understand the behavior of resorbable implants. Aliphatic polyesters are a class of polymers for which the erosion process is typically

modeled using a reaction–transport framework, where degradation is dictated by an autocatalytic hydrolysis mechanism and transport includes diffusion through the polymer matrix.^{9,26,31} Reaction–transport models have been applied to a range of aliphatic polyesters, including poly(orthoester), poly(4-methylcaprolactone), poly(caprolactone), poly(L-lactide) (PLLA), and poly(D,L-lactide-co-glycolide).³⁰ Hybrid models that employ stochastic reaction frameworks are mathematically complex but offer greater detail of transient polymer composition.^{4,27} Despite these and other efforts,^{2,10,24} previous models have not been extended to characterize the various kinetic factors that modulate by-product fate in the arterial environment. We have applied a reaction–transport framework to study how the outcome of material by-products released from a tissue-embedded BVS is governed by the hydrolytic degradation rate of the polymer, vascular remodeling, and arterial uptake.

We present a three-dimensional (3D) computational model of a BVS that is primarily composed of PLLA and fully embedded within an arterial wall. A volume of tissue surrounding the scaffold that undergoes cellular and extracellular remodeling post-implantation was represented as a distinct region with time-varying transport properties throughout the initial phases of erosion. PLLA degradation internal to the scaffold was modeled as a reaction–diffusion system, and transport of LA external to the scaffold was modeled as a reaction–convection–diffusion system coupled with equations governing luminal blood flow. Parametric studies were performed to quantify how local peak LA concentrations in tissue vary with PLLA degradation rate, temporal changes in LA transport properties due to tissue remodeling, and LA metabolism rate. Model

predictions indicate that the relative rates of tissue remodeling and polymer degradation modulate LA transport and suggest that a synchrony of these processes can minimize transient LA concentrations in tissue. Results further indicate that LA metabolism does not dramatically affect tissue concentrations and is an insignificant clearance mechanism relative to convective and diffusive transports. These observations add to our understanding of the means by which BVS degradation products are processed physiologically and the factors that may influence biological response to BVS therapy for coronary artery disease.

METHODS

A 3D computational model exploiting symmetric vessel characteristics was constructed based on the geometric and compositional characteristics of a representative bioresorbable vascular scaffold (BVS) (Abbott Vascular, Santa Clara, CA). The BVS implant is manufactured primarily from PLLA and consequently yields LA as a late degradation by-product. A 2D schematic of the computational domain utilized in this study depicts four geometric sub-domains: a longitudinal scaffold segment fully embedded within the arterial wall (S), a tissue healing zone (H) with transient transport properties at early implantation times, the remaining portion of the arterial wall (W), and the arterial lumen (L) (Fig. 1). A 3D geometry reflecting these sub-domains was constructed using SolidWorks (Dassault Systèmes),¹⁸ where the diameter and length of the lumen were 3×10^{-3} and 2.1×10^{-2} m, respectively, and the thickness of the healing zone and arterial wall were 1×10^{-4} and 1×10^{-3} m, respectively (Fig. 2a).

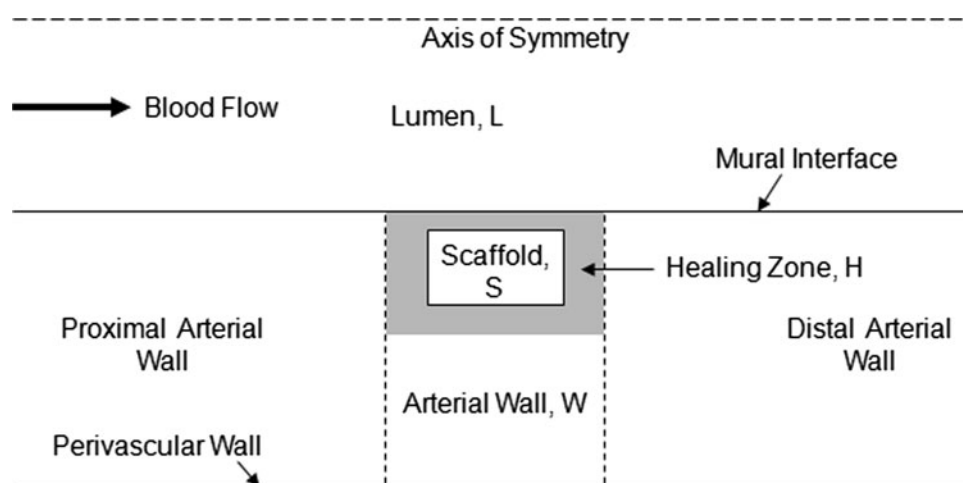


FIGURE 1. Schematic of the two-dimensional computational domain comprising a longitudinal scaffold segment (S) fully embedded within the arterial wall (W), a tissue healing zone (H) that undergoes marked changes in transport properties post-implantation, and the arterial lumen (L) (not to scale).

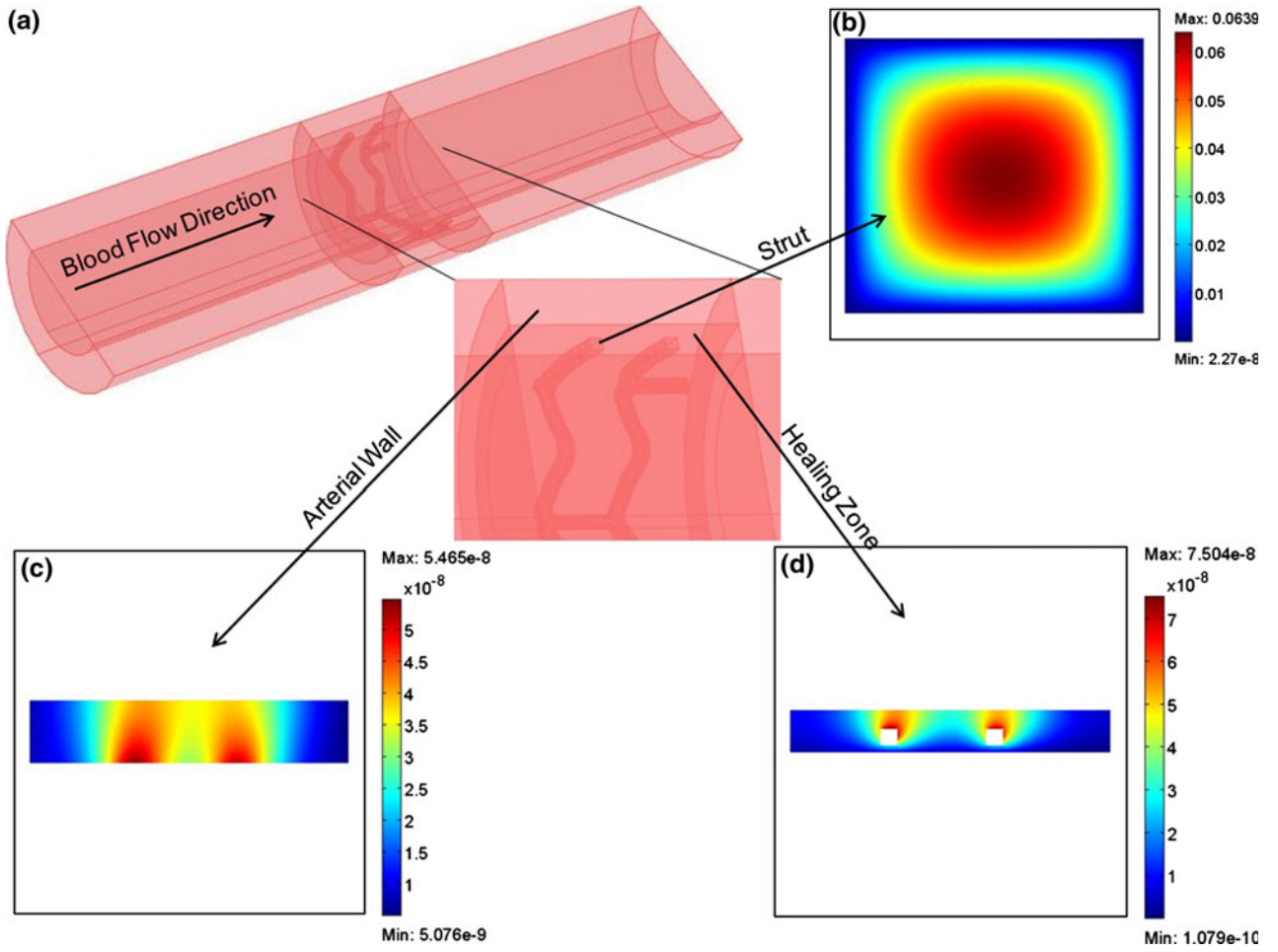


FIGURE 2. (a) Three-dimensional computational model of a fully erodible scaffold residing in the arterial wall. Blood is flowing in the lumen and the porous arterial wall. Insets show high magnification images of the strut (S), arterial wall (W), and healing zone (H). (b) LA concentration is maximal at the scaffold core and diminishes toward the boundary with the healing zone. (c, d) LA released from the scaffold is transported through H and W via diffusion and convection. LA concentration is the highest near the scaffold surface and reduces toward the perivascular wall. Hydrolytic degradation rate of $1 \times 10^{-7} \text{ s}^{-1}$, LA healing zone diffusivity change rate of $1 \times 10^{-7} \text{ s}^{-1}$, and LA metabolism rate of $1 \times 10^{-6} \text{ s}^{-1}$ were used in depicted simulation results. Color bars represent LA concentration for each inset.

Blood was considered as an incompressible, Newtonian fluid, and its flow through the lumen was assumed to be steady, laminar, and fully developed. Luminal flow was described by the momentum and continuity equations as follows:

$$\rho_L(\mathbf{u}_L \cdot \nabla \mathbf{u}_L) = -\nabla P_L + \mu_L \nabla^2 \mathbf{u}_L \quad (1)$$

$$\nabla \cdot \mathbf{u}_L = 0, \quad (2)$$

where \mathbf{u}_L , $\rho_L = 1060 \text{ kg m}^{-3}$; $\mu_L = 3.5 \times 10^{-3} \text{ Pa s}$, and P_L are, respectively, blood velocity, blood density, blood viscosity, and pressure within the luminal region.

Blood flow through both the porous arterial wall and healing zone were modeled using momentum and continuity equations:

$$\rho_W(\mathbf{u}_W \cdot \nabla \mathbf{u}_W) = -\nabla P_W + \left(\frac{1}{\varepsilon_W}\right) \mu_W \nabla^2 \mathbf{u}_W - \left(\frac{\mu_W}{k_W}\right) \mathbf{u}_W \quad (3)$$

$$\nabla \cdot \mathbf{u}_W = 0 \quad (4)$$

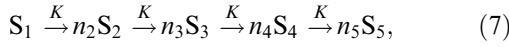
$$\rho_H(\mathbf{u}_H \cdot \nabla \mathbf{u}_H) = -\nabla P_H + \left(\frac{1}{\varepsilon_H}\right) \mu_H \nabla^2 \mathbf{u}_H - \left(\frac{\mu_H}{k_H}\right) \mathbf{u}_H \quad (5)$$

$$\nabla \cdot \mathbf{u}_H = 0, \quad (6)$$

where \mathbf{u}_W , $\rho_W = 1025 \text{ kg m}^{-3}$, $\mu_W = 7.2 \times 10^{-4} \text{ Pa s}$, P_W , $k_W = 1.43 \times 10^{-8} \text{ m}^2$ and $\varepsilon_W = 0.43$ are, respectively, transmural steady-state velocity, density, viscosity, pressure, Darcy's permeability, and porosity-characterizing

blood plasma flow in the arterial wall; \mathbf{u}_H , $\rho_H = 1025 \text{ kg m}^{-3}$, $\mu_H = 7.2 \times 10^{-4} \text{ Pa s}$, P_H , $k_H = 1.43 \times 10^{-8} \text{ m}^2$ and $\varepsilon_H = 0.43$ are, respectively, the transmural steady-state velocity, density, viscosity, pressure, Darcy's permeability, and porosity-characterizing blood plasma flow in the healing zone.²⁹

Poly(L-lactide) degradation was described by a reaction–diffusion model that considers autocatalyzed hydrolytic reactions. A simplified first-order degradation model was constructed based on the following reactions^{8,34}:



where S_i , n_i , and K are, respectively, the polymer species i ($i = 1, 2, 3, 4, 5$), the stoichiometric coefficient of species i , and the effective PLLA hydrolytic degradation rate that describes the conversion between molecular species. Initial polymer monodispersity was assumed in all simulations, implying the presence of a single high molecular weight (100 kDa) species before scaffold degradation. Although complete PLLA degradation would actually yield numerous distinct oligomers, the degradation process was modeled as a systematic evolution of four oligomers groups (S_1 – S_4) and eventually LA (S_5). These five species constituted a reduced representation of transient scaffold composition throughout the degradation and resorption processes (Table 1).

Autocatalysis caused by the formation of acid end-groups through each hydrolysis reaction was assumed to occur only within the scaffold. Oligomers in excess of the PLLA solubility limit (S_1 – S_4) were assumed to be static within the scaffold for all times, with only diffusion and transient release of LA (S_5) into the surrounding tissue.³³ Transient reaction–diffusion equations in the scaffold were considered as follows:

$$\frac{\partial C_1^S}{\partial t} = -KC_1 - K_a C_1 \sqrt{C_5} \quad (8)$$

$$\frac{\partial C_2^S}{\partial t} = n_2 KC_1 + n_2 K_a C_1 \sqrt{C_5} - KC_2 - K_a C_2 \sqrt{C_5} \quad (9)$$

TABLE 1. Range and average molecular weight of different species used to describe the degradation process of a fully erodible PLLA endovascular scaffold.

Species	Concentration (M)	M_w range (kDa)	Average M_w (kDa)
S_1	C_1	$80 \leq M_w < 120$	100
S_2	C_2	$40 \leq M_w < 80$	60
S_3	C_3	$10 \leq M_w < 40$	25
S_4	C_4	$0.1 \leq M_w < 10$	5
S_5	C_5	$0.1 \leq M_w$	0.1

$$\frac{\partial C_3^S}{\partial t} = \frac{n_3}{n_2} KC_2 + \frac{n_3}{n_2} K_a C_2 \sqrt{C_5} - KC_3 - K_a C_3 \sqrt{C_5} \quad (10)$$

$$\frac{\partial C_4^S}{\partial t} = \frac{n_4}{n_3} KC_3 + \frac{n_4}{n_3} K_a C_3 \sqrt{C_5} - KC_4 - K_a C_4 \sqrt{C_5} \quad (11)$$

$$\frac{\partial C_5^S}{\partial t} = \nabla \cdot (D_{C_5}^S \nabla C_5^S) + \frac{n_5}{n_4} KC_4 + \frac{n_5}{n_4} K_a C_4 \sqrt{C_5}, \quad (12)$$

where C_1 – C_5 , $D_{C_5}^S = 10^{-15} \text{ m}^2 \text{ s}^{-1}$, and $K_a = 7.5 \times 10^{-8} \sqrt{\text{mol m}^{-3} \text{ s}^{-1}}$ are, respectively, the concentration of chemical species S_1 – S_5 , the LA diffusion coefficient within the scaffold, and the autocatalytic degradation rate constant.¹⁰

The metabolism of LA in both the healing zone and the arterial wall was modeled as a first-order reaction.¹⁶ LA concentration inside the healing zone was modeled as transient reaction–diffusion–convection process:

$$\frac{\partial C_5^H}{\partial t} + \mathbf{u}_H \cdot \nabla C_5^H = \nabla \cdot (D_{C_5}^H \nabla C_5^H) - K_{m,H} C_5^H, \quad (13)$$

where $D_{C_5}^H$ and $K_{m,H}$ are, respectively, the LA diffusion coefficient and the metabolism rate within the healing zone.²¹ $D_{C_5}^H$ was modeled as an exponentially decaying transport property with an initial maximum value equal to the LA diffusion coefficient in the lumen ($D_{C_5}^L = 10^{-8} \text{ m}^2 \text{ s}^{-1}$) and a minimum value that is equal to the LA diffusion coefficient in the arterial wall ($D_{C_5}^W = 10^{-12} \text{ m}^2 \text{ s}^{-1}$). The transient value of $D_{C_5}^H$ was modeled as follows:

$$D_{C_5}^H - D_{C_5}^W = (D_{C_5}^L - D_{C_5}^W) e^{-\alpha t} \quad (14)$$

where α is the exponential constant that describes the transformation from blood-like to arterial-wall like behavior. LA concentration within the arterial wall was also modeled as a transient reaction–diffusion–convection process as follows:

$$\frac{\partial C_5^W}{\partial t} + \mathbf{u}_W \cdot \nabla C_5^W = \nabla \cdot (D_{C_5}^W \nabla C_5^W) - K_{m,W} C_5^W, \quad (15)$$

where $K_{m,W}$ is LA metabolism rate in the arterial wall. LA transport within the lumen was modeled as transient diffusion–convection process as follows:

$$\frac{\partial C_5^L}{\partial t} + \mathbf{u}_L \cdot \nabla C_5^L = \nabla \cdot (D_{C_5}^L \nabla C_5^L). \quad (16)$$

A fully developed, parabolic velocity profile with a mean velocity of 0.265 m s^{-1} was assumed at the luminal inlet.¹⁸ A transmural velocity boundary

condition was imposed in the normal direction of the mural interface on the basis of Kedem–Katchalsky equation,¹⁴ whereas a constant pressure boundary condition was imposed on the perivascular wall.²⁸ Symmetry boundary conditions were assigned both at the arterial wall inlet and outlet, and along the vessel center-line.

For species evolution and transport, S_1 with unit concentration was the initially imposed within the scaffold sub-domain. Flux continuity of the mobile species S_5 was maintained at the scaffold surface, healing zone–arterial wall interface, and the mural interface, while a convective flux boundary condition was also imposed at the perivascular wall. A zero-concentration condition was assumed at the lumen inlet, as upstream species transport is largely prevented by luminal flow.^{3,7} Conversely, downstream species transport is flow assisted and assumed to be a convection-dominated process, motivating the use of a convective flux boundary condition at the lumen outlet.³⁵

The computational domain was meshed using 102,845 tetrahedral elements, with a relative tolerance of 10^{-5} required for solution convergence. An adaptive meshing procedure was used to create a continuous mesh with maximum density at the scaffold surface and minimum density along the center-line of the lumen, facilitating high-fidelity results in the tissue regions of interest. The finite-element framework (COMSOL MultiphysicsTM) yielded a mesh-independent solution that was defined as a less than 0.1% relative change in C_1 within the scaffold at 24 months following successive adaptive refinements.

RESULTS

Our computational model provided converged solutions for the spatial and temporal distributions of BVS by-products over a wide range of kinetic parameters characterizing PLLA degradation, arterial remodeling, LA transport, and metabolism. The spatial distribution of LA within the scaffold was maximal at the core and decreased toward the boundary with the healing zone for all times, confirming diffusion-mediated LA transport within the scaffold sub-domain (Fig. 2b). However, a substantial amount of LA was transported by transmural convection both in the healing zone and the arterial wall, evidenced by a greater increase in LA concentration in the radial as opposed to axial direction within both sub-domains (Figs. 2c and 2d). These trends are a consequence of the simulated average transmural blood velocity ($1.64 \times 10^{-8} \text{ m s}^{-1}$), which is consistent with the previously reported experimental results attained within rabbit aortic walls ($1.78 \times 10^{-8} \text{ m s}^{-1}$).²⁰ Moreover, the LA concentration was evidently higher in the distal

compared with proximal regions of both the scaffold and healing zone, indicating that blood flow affects transport in these sub-domains.

The simulated autocatalytic degradation process resulted in a nonlinear decrease of the number-averaged molecular weight (M_n) of the insoluble scaffold species post-implantation (Fig. 3a). For a given set of parameters, our model predictions correlate well ($R = 0.99$, $p < 0.05$) to *in vivo* measurements of BVS scaffold degradation,²² providing support for the employed degradation model and analyzed range of degradation rates. When the PLLA hydrolytic degradation rate (K) was $7.5 \times 10^{-8} \text{ s}^{-1}$, the scaffold underwent a rapid reduction of M_n in first 12 months, followed by period of gradual decline to approximately 3% of the initial value after 2 years. Transient scaffold molecular distributions (insets in Fig. 3a) demonstrate that defined chemical species groups are present in various concentrations through the degradation process, with a relatively high concentration of LA within the scaffold at early times (<12 months post implantation). Early accumulation of LA within the scaffold implies that the generation rate exceeds the diffusion-mediated transport rate, a phenomenon that is in agreement with previously reported computational results.²⁵

An order of magnitude variation in K dramatically affects scaffold M_n over a two-year period (Fig. 3b). M_n is reduced by over 40% within 1 month under the fastest K ($5 \times 10^{-7} \text{ s}^{-1}$), while an order of magnitude decrease in K results in less than 1% M_n reduction at the same time point. The significant model response to variation in K is an expected characteristic of autocatalytic polymers such as PLLA, where trace levels of LA within the material can substantially accelerate degradation.

The transient LA concentration within the scaffold is consistently orders of magnitude greater than that in the lumen or surrounding arterial wall, suggesting that the arterial environment behaves as a sink for evolved by-products. The healing zone is a predefined region of arterial tissue (10% of arterial wall thickness) surrounding the scaffold that is postulated to undergo changes in transport properties as a consequence of tissue remodeling. As a consequence of proximity to the scaffold, LA concentrations are consistently higher in the healing zone than in the arterial wall (Fig. 3c), implying that local tissue is at a greatest risk of by-product accumulation despite initially accelerated transport associated with incomplete healing. Transient LA concentrations within the healing zone and the arterial wall follow similar trends for a prescribed K . However, a strong dependence of the time course and nature of these trends on K is observed. Under the fastest K ($5 \times 10^{-7} \text{ s}^{-1}$), LA concentration sharply increases over the first month, but is essentially cleared

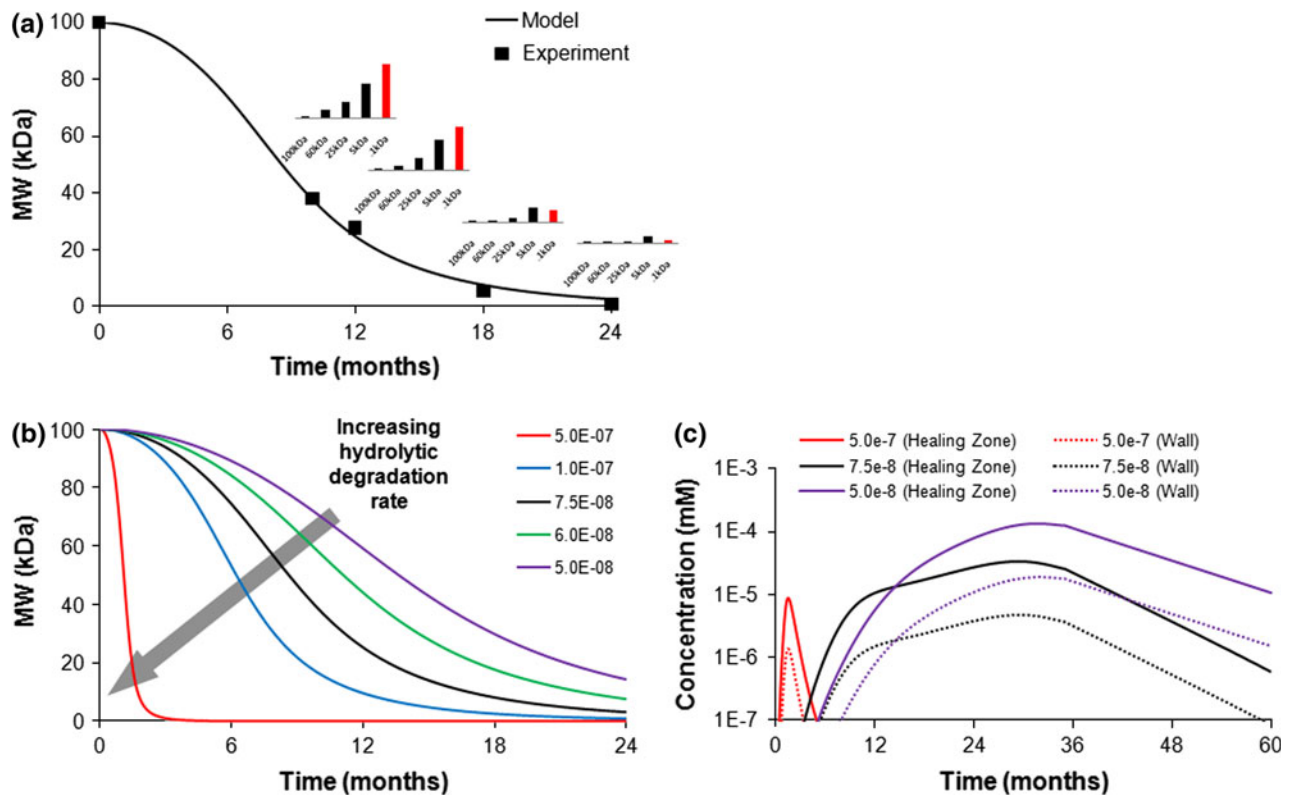


FIGURE 3. (a) Simulated number averaged molecular weight change of insoluble scaffold species (smooth line) as a function of implantation time agree with previously reported experimental measurements of BVS.²² Insets depict the relative concentration of the insoluble oligomer species (black bars) and soluble species (red bars) within the scaffold domain throughout the degradation process. (b) The number averaged molecular weight of the scaffold as a function of time for various hydrolytic degradation rates. Increased hydrolytic degradation rate (K) leads to a markedly faster reduction in scaffold number-averaged molecular weight. (c) LA concentration within the healing zone and arterial wall over 5 years post-implantation for various K . At all times, the LA concentration is approximately an order of magnitude greater in the healing zone compared to the arterial wall. A hydrolytic degradation rate of $7.5 \times 10^{-8} \text{ s}^{-1}$ was used for (a). A LA healing zone diffusivity change rate of $1 \times 10^{-7} \text{ s}^{-1}$ and LA metabolism rate of $1 \times 10^{-6} \text{ s}^{-1}$ were used in all illustrated simulation results (a–c).

by one year. For intermediate K ($7.5 \times 10^{-8} \text{ s}^{-1}$), there is a moderately sharp increase in LA concentration over the first 10 months followed by a period of sustained concentration that persists until approximately 29 months. When K is the lowest ($5 \times 10^{-8} \text{ s}^{-1}$), a gradual increase of LA concentration occurs over a period of 32 months followed by a protracted decline thereafter.

The peak concentration of LA within the healing zone (C_{\max}) varied nonlinearly with K (Fig. 4a). Trends indicate that C_{\max} initially has a strong negative dependence on K until a critical limit is surpassed. At K exceeding $1.4 \times 10^{-7} \text{ s}^{-1}$, faster degradation results in slightly greater LA accumulation within local tissue. The time point at which C_{\max} occurs (t_{\max}) is monotonically reduced with faster degradation, and abruptly drops from over 2 years to less than 6 months post-implantation when K approaches the critical limit of $1.4 \times 10^{-7} \text{ s}^{-1}$ (Fig. 4b). The temporal change in LA diffusivity within the healing zone reflects the transition from lumen-like to arterial wall-like transport

properties as local tissue is remodeled. An increase in the exponential rate constant governing diffusivity (α) leads to a higher C_{\max} , implying that transient transport properties adjacent to a scaffold can influence LA accumulation (Fig. 4c). The values for t_{\max} are nearly constant for $\alpha < 5.25 \times 10^{-8} \text{ s}^{-1}$, suggesting that clearance within this regime is not limited by transport through the healing zone (Fig. 4d). However, a more complex dependence is observed when $\alpha \geq 7.5 \times 10^{-8} \text{ s}^{-1}$, as peak LA levels are not only orders of magnitude higher as compared to lower rates, but also occur at substantially later times post-implantation.

The relative rates of transport property change within the healing zone and PLLA hydrolytic degradation (α/K) show bi-modal governance of C_{\max} (Fig. 5a). When $\alpha/K < 1$, the resultant C_{\max} is always less than the value observed when $\alpha/K = 1$. Conversely, when $\alpha/K > 1$, C_{\max} is comparatively elevated. These trends suggest that LA is most effectively cleared from local tissue when the rate of scaffold degradation

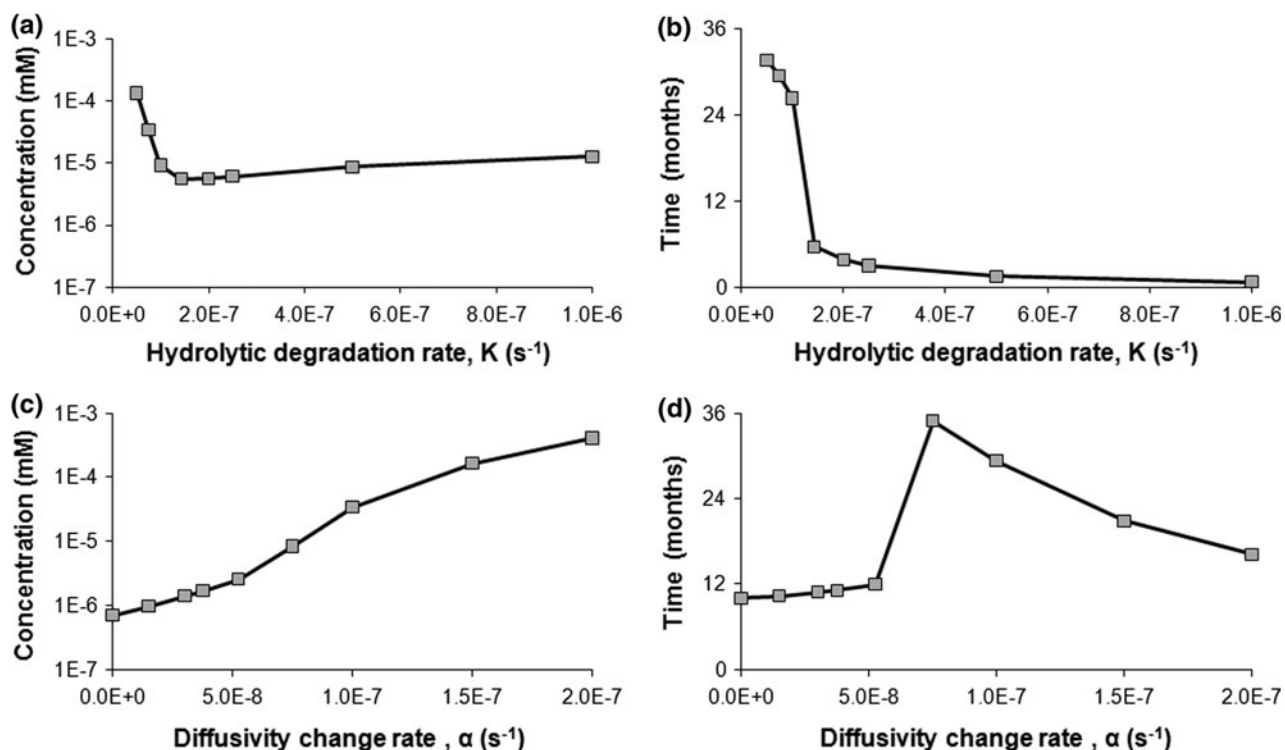


FIGURE 4. (a, b) Hydrolytic degradation rate (K) modulated both peak LA concentration within the healing zone (C_{max}) and the time after implantation (t_{max}) at which the said concentration occurred. Dependence of C_{max} on K follows U-shaped kinetics, whereas t_{max} monotonically decreases with K . (c, d) Increased diffusivity change rate (α) within the healing zone led to increased C_{max} , but only affected t_{max} at comparatively high values ($\alpha \geq 1 \times 10^{-7} s^{-1}$). A LA metabolism rate of $1 \times 10^{-6} s^{-1}$ was used in all illustrated simulation results.

is greater than the rate of conversion from a lumen-like to an arterial wall-like domain. The operative α/K also modulates t_{max} , although in a less uniform manner (Fig. 5b). In general, $\alpha/K < 1$ results in the peak concentrations occurring at earlier times post-implantation, while $\alpha/K \geq 1$ leads to relatively greater t_{max} .

In all simulations, LA metabolism rates within the healing zone ($K_{m,H}$) and arterial wall ($K_{m,W}$) were set to equal values ($K_{m,W} = K_{m,H} = K_m$). Order of magnitude variations in K_m (1×10^{-7} – $1 \times 10^{-5} s^{-1}$) had an insignificant effect on both the resultant C_{max} and t_{max} (Figs. 6a and 6b). Only an extreme metabolic rate of $1 \times 10^{-3} s^{-1}$ influenced transient LA levels in local tissue, with approximately a 70% reduction in C_{max} compared to lower rates.

DISCUSSION

The ultimate fate of implant-derived chemical species is subject to a complex array of factors that often preclude delineation through traditional experimentation. Even when carefully designed bench-top experiments provide characterizations of material degradation and erosion, results do not always reflect *in vivo* performance. Prediction of implant behavior and

degradant species fate *in vivo* is confounded by variations in governing processes such as species generation/release rates, diffusive/convective transport, and metabolism, all of which are subject to change based on precise implantation site, implant composition and properties, and patient status. While BVS have the potential to improve upon current treatment options for ischemic artery disease, we must understand the numerous factors that will dictate device safety and efficacy. Complete scaffold erosion could not only potentially mitigate long-term risks that limit permanent alternatives, but also introduce new concerns with injurious by-product accumulation in local arterial tissue.

It is critical to account for the transient levels of LA that accumulate in local tissue throughout the implant lifetime to predict the safety of BVS composed of PLLA. Convective and diffusive transport coupled with metabolic elimination governs naturally fluctuating LA tissue levels in normal physiologic scenarios. While the same clearance mechanisms would be operative following scaffold implantation, high transient LA concentrations could arise in local tissue during the erosion process and create an acidic environment.^{23,32} BVS evaluation, both in terms of functional performance and safety, requires extensive *in vivo* studies that

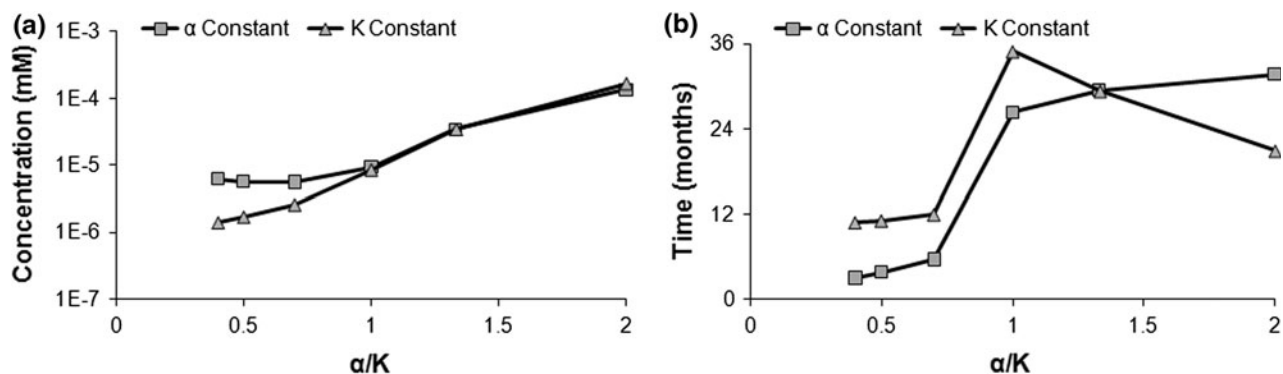


FIGURE 5. The ratio of the diffusivity change rate within the healing zone (α) to the hydrolytic degradation rate of the scaffold (K) was varied between 0.4 and 2 by altering either rate constant in isolation. (a) The peak LA concentration within the healing zone (C_{\max}) generally had a positive dependence on α/K regardless of which rate was varied. (b) The time at which C_{\max} occurs (t_{\max}) showed a near binary dependence on α/K . When $\alpha/K < 1$, t_{\max} was less than 12 months for all tested cases; when $\alpha/K \geq 1$, t_{\max} was comparatively longer (21–35 months). A LA metabolism rate of $1 \times 10^{-6} \text{ s}^{-1}$ was used in all illustrated simulation results.

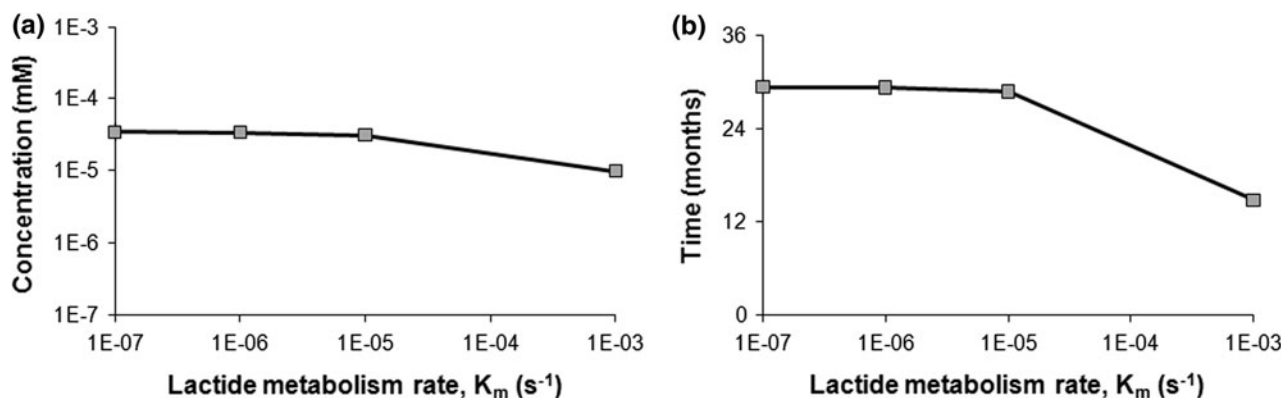


FIGURE 6. Metabolism of LA is a secondary clearance mechanism from tissue as compared to convective/diffusive transport. (a, b) The peak LA concentration in the healing zone (C_{\max}) and the time at which it occurs (t_{\max}) were largely independent of metabolism (K_m), with an effect observed only at the maximal simulated rate ($K_m = 1 \times 10^{-3} \text{ s}^{-1}$). A hydrolytic degradation rate of $7.5 \times 10^{-8} \text{ s}^{-1}$ and a LA healing zone diffusivity change rate of $1 \times 10^{-7} \text{ s}^{-1}$ were used in all illustrated simulation results.

measure LA generation, release, and concentration in tissue over the implant lifetime—these experiments are conducted at high cost and on the timescale of years. Computational modeling offers an efficient and complementary framework for critical implant assessment and facilitates both understanding and prediction of BVS behavior.

In an intriguing fashion, our results predict that the kinetic rates of PLLA hydrolysis (K) and the local change in arterial diffusivity associated with tissue remodeling (α) dominate over metabolism (K_m) in determining the peak local tissue LA concentrations (C_{\max}). Degradation kinetics modulated C_{\max} in a complex fashion, with a trend inflection observed at an intermediate rate within the analyzed parametric space (Fig. 4a). The trend results from an interplay between polymer degradation and arterial healing rates, which is further revealed upon direct analyses of the dimensionless constant α/K (Fig. 5a). LA clearance from local

tissue is favored at low α/K , where degradation dominates and is far faster than the reduction in transport associated with healing. The rate of transformation of local tissue from a temporary clot immediately following implantation (lumen-like) to a stable cellularized substrate (arterial wall-like), therefore cannot be overlooked when changes in the material structure and arterial transport properties are on similar timescales. Synchrony between the degradation and healing processes emerges as a design guideline that can be applied to BVS, but obviously must be balanced against the need for physical persistence of the scaffold at the implantation site in order to achieve the therapeutic effect.^{1,5}

Our simulations predict that extreme variations in LA metabolism will have a negligible effect on local tissue concentrations, suggesting that convective and diffusive transport are the primary clearance mechanisms within the arterial environment (Fig. 6a). Because scaffold lifetime is presumably independent of

LA metabolism within the tissue, our results imply that patient-specific variations in metabolic activity can largely be ignored in designing BVS prototypes for clinical use. Conversely, the change in LA transport that accompanies tissue transformation is a strong determinant of scaffold safety that may implicate more application-specific variation driven by deployment protocols and operator techniques.

STUDY LIMITATIONS AND FUTURE WORK

As with most computational studies, results and drawn inferences become all the more valuable when coupled with experimental and/or clinical data. Previous studies provided qualitative assessment of the transient tissue response following BVS implantation in the pig coronary artery.²² Based on these studies, we were able to assume reasonable spatial dimensions for the simulated healing zone and confidently treat this region as being geometrically stable throughout the simulation time. However, there is no reported study of chemical species transport properties within the arterial wall and over time. In our model, we assumed that healing zone transport properties would transition from blood-like to arterial-wall like in a manner that is independent of local physiological factors. This is not necessarily the case *in vivo*—local LA concentration could potentially impact tissue remodeling and thus transient transport properties. In lieu of definitive experimental data, our approach was to conduct parametric analyses to predict how the kinetics of local tissue transformation will modulate LA transport and accumulation. Due to the multitude of simulated physicochemical processes, technical challenges in related experiments, and long simulated time periods (~5 years), some model assumptions related to the healing zone preclude experimental validation and should be carefully considered when interpreting computational results.

While important in modeling flow-mediated transport in the arterial lumen, previous studies suggest that blood pulsatility minimally influences the chemical species transport within the arterial wall.^{17,35} Histology of the main coronary artery of pigs following implantation of BVS indicates that scaffolds are fully covered by a fibromuscular neointima after only 28 days.²² As this time period represents just an early stage of the developed computational model (60 months), we treated the scaffold as a fully embedded implant through the entire simulation time and discarded the pulsatile nature of luminal flow. Nevertheless, our developed framework paves way for future studies that account for various levels of scaffold embedding and/or blood pulsatility.

Although PLLA degradation model proposed in this study can match experimental data for a given set of parameters (Fig. 3a), this model featured a limited number of oligomer/monomer species generated through abbreviated degradation steps governed by a single rate constant. Scaffold degradation could be more accurately modeled with either (i) a probabilistic modifier of the degradation rate constant to describe chain scission from a longer chain into multiple smaller chains or (ii) a stochastic model governed by the intrinsic degradation rate constant that allows for generation of all possible oligomers throughout the degradation process. Moreover, we assumed that the scaffold was initially a monodisperse polymer matrix with a normalized concentration of the single species. In the tissue domains, LA metabolism was modeled as a single-step process governed by a single rate K_m , even though the actual metabolic pathway is considerably more complex. The assumptions driving the employed degradation and metabolism models enable management of computational cost and facilitate parametric analyses of multiple key processes.

Future study should include more realistic models of degradation and increasingly be based on system-specific experimental data. Because of our model assumptions, the reported by-product concentrations cannot be directly used to predict clinical safety, but instead enable elucidation of deterministic processes and relationships among various kinetic parameters. While limitations and assumptions must be taken into account, computational modeling provides a cost-effective approach to gain new insight on the interplay between tissue remodeling, polymer degradation, and metabolic clearance in determining by-product retention and distribution within arterial tissue.

CONCLUSIONS

Our study suggests that tissue remodeling and polymer degradation kinetics modulate LA accumulation within adjacent arterial tissue in the case of a tissue-embedded, BVS composed of PLLA. On the other hand, peak LA concentrations were insensitive to large variation in the tissue metabolic rate, suggesting that metabolism is a secondary by-product clearance mechanism compared to diffusive and convective transport. Synchrony between rates of remodeling and degradation is predicted to minimize peak LA levels in local tissue over the scaffold lifetime. As BVS are increasingly considered for the treatment of coronary artery disease, insights on the production and tissue retention of degradation by-products can help predict clinical performance and provide a basis for iterative device design.

ACKNOWLEDGMENTS

This study was supported by the NIH grant (R01 GM-49039) to ERE and the National Science Foundation/EPSCoR Grant (EPS-0903795) to TS. The authors thank Tecplot, Inc. for generously providing software licenses for data visualization.

REFERENCES

- ¹Adachi, T., Y. Osako, M. Tanaka, M. Hojo, and S. J. Hollister. Framework for optimal design of porous scaffold microstructure by computational simulation of bone regeneration. *Biomaterials* 27(21):3964–3972, 2006.
- ²Antheunis, H., J.-C. van der Meer, M. de Geus, W. Kingma, and C. E. Koning. Improved mathematical model for the hydrolytic degradation of aliphatic polyesters. *Macromolecules* 42(7):2462–2471, 2009.
- ³Balakrishnan, B., J. F. Dooley, G. Kopia, and E. R. Edelman. Intravascular drug release kinetics dictate arterial drug deposition, retention, and distribution. *J. Control Release* 123(2):100–108, 2007.
- ⁴Chen, Y., S. Zhou, and Q. Li. Mathematical modeling of degradation for bulk-erosive polymers: applications in tissue engineering scaffolds and drug delivery systems. *Acta Biomater.* 7(3):1140–1149, 2011.
- ⁵Chen, Y., S. Zhou, and Q. Li. Microstructure design of biodegradable scaffold and its effect on tissue regeneration. *Biomaterials* 32(22):5003–5014, 2011.
- ⁶Colombo, A., and E. Karvouni. Biodegradable stents: “fulfilling the mission and stepping away”. *Circulation* 102(4):371–373, 2000.
- ⁷Deen, W. M. Analysis of Transport Phenomena. New York: Oxford University Press, 597 pp, 1998.
- ⁸Flory, P. J. Principles of Polymer Chemistry. Ithaca: Cornell University Press, 688 pp, 1953.
- ⁹Göpferich, A. Mechanisms of polymer degradation and erosion. *Biomaterials* 17(2):103–114, 1996.
- ¹⁰Han, X., and J. Pan. Polymer chain scission, oligomer production and diffusion: a two-scale model for degradation of bioresorbable polyesters. *Acta Biomater.* 7(2):538–547, 2011.
- ¹¹Higo, T., Y. Ueda, J. Oyabu, K. Okada, M. Nishio, A. Hirata, K. Kashiwase, N. Ogasawara, S. Hirotsu, and K. Kodama. Atherosclerotic and thrombotic neointima formed over sirolimus drug-eluting stent: an angiographic study. *JACC Cardiovasc. Imaging* 2(5):616–624, 2009.
- ¹²Iakovou, I., T. Schmidt, E. Bonizzoni, L. Ge, G. M. Sangiorgi, G. Stankovic, F. Airoldi, A. Chieffo, M. Montorfano, M. Carlino, I. Michev, N. Corvaja, C. Briguori, U. Gerckens, E. Grube, and A. Colombo. Incidence, predictors, and outcome of thrombosis after successful implantation of drug-eluting stents. *J. Am. Med. Assoc.* 293(17):2126–2130, 2005.
- ¹³Jagur-Grodzinski, J. Polymers for tissue engineering, medical devices, and regenerative medicine. Concise general review of recent studies. *Polym. Adv. Technol.* 17(6):395–418, 2006.
- ¹⁴Kedem, O., and A. Katchalsky. Thermodynamic analysis of the permeability of biological membranes to non-electrolytes. *Biochim. Biophys. Acta* 27:229–246, 1958.
- ¹⁵Kimura, T., K. Abe, S. Shizuta, K. Odashiro, Y. Yoshida, K. Sakai, K. Kaitani, K. Inoue, Y. Nakagawa, H. Yokoi, M. Iwabuchi, N. Hamasaki, H. Nosaka, and M. Nobuyoshi. Long-term clinical and angiographic follow-up after coronary stent placement in native coronary arteries. *Circulation* 105(25):2986–2991, 2002.
- ¹⁶Kobayashi, M., I. Fujita, S. Itagaki, T. Hirano, and K. Iseki. Transport mechanism for L-lactic acid in human myocytes using human prototypic embryonal rhabdomyosarcoma cell line (RD cells). *Biol. Pharm. Bull.* 28(7):1197–1201, 2005.
- ¹⁷Kolachalama, V. B., E. G. Levine, and E. R. Edelman. Luminal flow amplifies stent-based drug deposition in arterial bifurcations. *PLoS One* 4(12):e8105, 2009.
- ¹⁸Kolachalama, V. B., A. R. Tzafirri, D. Y. Arifin, and E. R. Edelman. Luminal flow patterns dictate arterial drug deposition in stent-based delivery. *J. Control Release* 133(1):24–30, 2009.
- ¹⁹Leenslag, J. W., A. J. Pennings, R. R. M. Bos, F. R. Rozema, and G. Boering. Resorbable materials of poly(L-lactide): VII. In vivo and in vitro degradation. *Biomaterials* 8(4):311–314, 1987.
- ²⁰Meyer, G., R. Merval, and A. Tedgui. Effects of pressure-induced stretch and convection on low-density lipoprotein and albumin uptake in the rabbit aortic wall. *Circ. Res.* 79(3):532–540, 1996.
- ²¹Miller, R. A., J. M. Brady, and D. E. Cutright. Degradation rates of oral resorbable implants (polylactates and polyglycolates): rate modification with changes in PLA/PGA copolymer ratios. *J. Biomed. Mater. Res.* 11(5):711–719, 1977.
- ²²Onuma, Y., P. W. Serruys, L. E. L. Perkins, T. Okamura, N. Gonzalo, H. M. Garcia-Garcia, E. Regar, M. Kamberi, J. C. Powers, R. Rapoza, H. van Beusekom, W. van der Giessen, and R. Virami. Intracoronary optical coherence tomography and histology at 1 month and 2, 3, and 4 years after implantation of everolimus-eluting bioresorbable vascular scaffolds in a porcine coronary artery model. *Circulation* 122(22):2288–2300, 2010.
- ²³Pamula, E., and E. Menaszek. In vitro and in vivo degradation of poly(L-lactide-co-glycolide) films and scaffolds. *J. Mater. Sci. Mater. Med.* 19(5):2063–2070, 2008.
- ²⁴Perale, G., P. Arosio, D. Moscatelli, V. Barri, M. Müller, S. Maccagnan, and M. Masi. A new model of resorbable device degradation and drug release: transient 1-dimension diffusion model. *J. Control Release* 136(3):196–205, 2009.
- ²⁵Prabhu, S., and S. Hossainy. Modeling of degradation and drug release from a biodegradable stent coating. *J. Biomed. Mater. Res. A* 80A(3):732–741, 2007.
- ²⁶Siepmann, J., K. Elkharraz, F. Siepmann, and D. Klose. How autocatalysis accelerates drug release from PLGA-based microparticles: a quantitative treatment. *Biomacromolecules* 6(4):2312–2319, 2005.
- ²⁷Soares, J. S., and P. Zunino. A mixture model for water uptake, degradation, erosion and drug release from poly-disperse polymeric networks. *Biomaterials* 31(11):3032–3042, 2010.
- ²⁸Sun, N., N. Wood, A. Hughes, S. Thom, and X. Xu. Fluid-wall modelling of mass transfer in an axisymmetric stenosis: effects of shear-dependent transport properties. *Ann. Biomed. Eng.* 34(7):1119–1128, 2006.
- ²⁹Tada, S., and J. Tarbell. Fenestral pore size in the internal elastic lamina affects transmural flow distribution in the artery wall. *Ann. Biomed. Eng.* 29(6):456–466, 2001.

- ³⁰Thombre, A. G., and K. J. Himmelstein. A simultaneous transport-reaction model for controlled drug delivery from catalyzed bioerodable polymer matrices. *AIChE J.* 31(5):759–766, 1985.
- ³¹von Burkersroda, F., L. Schedl, and A. Göpferich. Why degradable polymers undergo surface erosion or bulk erosion. *Biomaterials* 23(21):4221–4231, 2002.
- ³²von Recum, H. A., R. L. Cleek, S. G. Eskin, and A. G. Mikos. Degradation of polydispersed poly(L-lactic acid) to modulate lactic acid release. *Biomaterials* 16(6):441–447, 1995.
- ³³Wang, Y., J. Pan, X. Han, C. Sinka, and L. Ding. A phenomenological model for the degradation of biodegradable polymers. *Biomaterials* 29(23):3393–3401, 2008.
- ³⁴Weir, N. A., F. J. Buchanan, J. F. Orr, and G. R. Dickson. Degradation of poly-L-lactide. Part 1: in vitro and in vivo physiological temperature degradation. *Proc. IME H. J. Eng. Med.* 218(5):307–319, 2004.
- ³⁵Yang, N., and K. Vafai. Modeling of low-density lipoprotein (LDL) transport in the artery—effects of hypertension. *Int. J. Heat Mass Transf.* 49(5–6):850–867, 2006.